THE JOURNAL OF PHYSICAL CHEMISTRY C

Article

pubs.acs.org/JPCC

Ag-Nanoparticle-Decorated SiO_2 Nanospheres Exhibiting Remarkable Plasmon-Mediated Photocatalytic Properties

Kuang-Hsiu Chen,[†,⊥] Ying-Chih Pu,[‡,⊥] Kao-Der Chang,[§] Yi-Fan Liang,[†] Chia-Ming Liu,[§] Jien-Wei Yeh,[†] Han-C. Shih,*[,†,∥] and Yung-Jung Hsu*[,‡]

[†]Department of Materials Science and Engineering, National Tsing Hua University, 101, Section 2, Kuang-Fu Road, Hsinchu 30013, Taiwan, ROC

[‡]Department of Materials Science and Engineering, National Chiao Tung University, 1001 University Road, Hsinchu 30010, Taiwan, ROC

[§]Nano Technology Research Center, Industrial Technology Research Institute, 195, Section 4, Chung Hsing Road, Chutung, Hsinchu 31040, Taiwan, ROC

[∥]Department of Chemical and Materials Engineering, Chinese Culture University, 55, Hwa-Kang Road, Yang-Ming-Shan, Taipei 11114, Taiwan, ROC

ABSTRACT: We demonstrated for the first time that Ag-nanoparticle-decorated SiO_2 nanospheres (NSs) may display noticeable photocatalytic activities upon surface plasmon resonance (SPR) excitation. The samples were prepared by reacting SiO_2 NSs with $AgNO_3$ in the seed-mediated growth process, from which the Ag particle size and decoration density can be readily controlled. The dependence of the SPR-mediated photocatalytic performance of Ag-decorated SiO_2 NSs on the Ag morphology was investigated and presented. The as-prepared Ag-decorated SiO_2 NSs showed a significantly red shifted and relatively broad SPR absorption when compared with the individually dispersed Ag nanoparticles. Owing to the considerably broad SPR absorption that spanned from the visible to the near-infrared region, Ag-decorated SiO_2 NSs surpassed N-doped P-25 TiO_2 powder and individually dispersed Ag nanoparticles in photocatalytic activity, demonstrating their potential as an active photocatalyst in nearly all the current photocatalysis applications. Furthermore, the result of performance evaluation under natural sunlight shows that the present Ag-decorated SiO_2 NSs can be used as highly efficient photocatalysts that may practically harvest energy from sunlight. The current study provides a new paradigm for designing plasmonic metal nanostructures that can effectively absorb the entire solar spectrum and beyond for solar fuel generation.

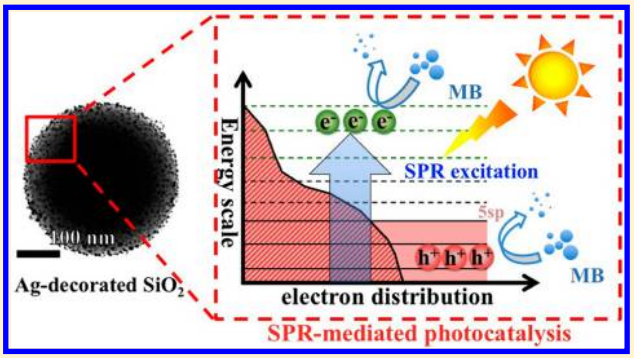

INTRODUCTION

The quantity of energy in the form of natural sunlight that strikes the Earth in 1 day is greater than the total annual worldwide energy consumption.[1] With growing energy and environmental concerns, there is currently a rising demand for development of novel solar energy conversion technologies. Among them, photocatalysis is of particular interest because of its capability of converting solar energy into chemical energy.[2,3] The most widely used semiconductor photocatalysts are metal oxides such as TiO_2, which absorbs ultraviolet only owing to its large band-gap energy. To practically harvest energy from sunlight, that is, to make use of visible light for photocatalysis, TiO_2 can be doped with suitable elements as such to create an additional electronic level in the energy gap.[4] In fact, a great deal of research attention is nowadays devoted to the development of photocatalysts that operate under visible light illumination. It has been extensively demonstrated that II−VI semiconductors, such as CdS[5,6] and CdSe,[7,8] exhibit fascinating photocatalytic activities upon visible light irradiation. The cytotoxicity of cadmium, however, limits the practical applications of such materials as photocatalysts. Hence, preparation of nontoxic and efficient visible-light-driven photocatalysts from more facile, mild synthetic approaches is becoming essential to move the field of photocatalysis technology forward.

With the capability of surface plasmon resonance (SPR) absorption in the visible range, Ag nanoparticles have been recently proposed as a novel photocatalyst for degradation of organic pollutants.[9−12] Since the SPR of Ag energizes the conduction electrons and excites them from the outermost 5sp bands to higher-energy states, there is a great probability that these electrons can participate in chemical reactions.[10,11]

Received: July 3, 2012
Revised: August 9, 2012
Published: August 11, 2012

   dx.doi.org/10.1021/jp306555j | J. Phys. Chem. C 2012, 116, 19039−19045

Simultaneously, the abundant holes left in the 5sp bands exhibit strong oxidizing power, which can also drive oxidation reactions to achieve photocatalysis. The effective generation of charge carriers under visible light illumination thus renders Ag nanoparticles potentially useful in a wide range of applications, such as solar fuel production and environmental remediation. In general, the oscillation frequency of the SPR of Ag is strongly sensitive to particle size and shape as well as the medium surrounding them. It has been reported that the SPR absorption of Ag nanoparticles may be greatly tailored after the introduction of SiO_2. For example, the SPR line shape of Ag-nanoparticle-coated SiO_2 nanospheres (NSs) can be delicately tuned by changing the thickness of Ag and the size of SiO_2.[13] The tunable SPR property for Ag may affect the charge carrier generation to further their performance in photocatalysis. Besides, the structural feature of Ag-coated SiO_2 NSs is advantageous to photocatalysis applications. First, the coated Ag nanoparticles are firm and stable during the photocatalytic operation, and exhibit high activity due to the small size. Second, the supported SiO_2 NSs have a relatively large size and can be easily recycled by filtration or centrifugation. As a result, Ag-coated SiO_2 NSs offer great promise as an efficient visible-light-responsive photocatalyst.

To date, several studies have described the preparation of Ag-coated SiO_2 NSs from methods, such as surface seeding,[14] electroless plating,[15−17] surface precipitation reaction,[18−22] and layer-by-layer self-assembly.[23] Most of them required surface functionalization to guide Ag coating, which makes control over Ag particle size and coating density difficult to achieve.[14−17,21,22] There is also little discussion in the literature regarding the photocatalytic performance of Ag-coated SiO_2 NSs, and its dependence on the morphology of Ag is rarely reported. Therefore, a systematic study on this topic is crucial to both the fundamental understanding and the practical applications for Ag/SiO_2 composite systems. In this work, we developed a facile seed-mediated growth approach to fabricate Ag-nanoparticle-decorated SiO_2 NSs without the use of surface functionalization. The Ag particle size and decoration density of the products can be readily controlled by adjusting the pH value of the seed reaction solution. We analyzed the details of seed-mediated growth, discussed the optical properties of the samples, and investigated for the first time the SPR-mediated photocatalytic performance of Ag-decorated SiO_2 and its dependence on Ag morphology. The as-prepared Ag-decorated SiO_2 NSs showed a significantly red shifted and relatively broad SPR absorption when compared with the individually dispersed Ag nanoparticles. Because of the considerably broad SPR absorption that spanned from the visible to the near-infrared region, abundant charge carriers were generated in Ag-decorated SiO_2 NSs, making them highly desirable for photocatalysis applications. As compared with N-doped P-25 TiO_2 powder and individually dispersed Ag nanoparticles, the as-prepared Ag-decorated SiO_2 NSs exhibited superior photocatalytic performance under white light illumination, demonstrating their potential as an active photocatalyst in nearly all the current photocatalysis applications. Furthermore, the photocatalytic performance under natural sunlight was also tested, and the result shows that the present Ag-decorated SiO_2 NSs can be used as highly efficient photocatalysts that may practically harvest energy from sunlight.

EXPERIMENTAL SECTION

Chemicals. All chemicals were of analytical grade and used without further purification.

Preparation of SiO_2 NSs. SiO_2 NSs were prepared according to the Stöber method, which involves the ammonia-catalyzed hydrolysis and condensation of tetraethyl orthosilicate ($Si(OC_2H_5)_4$, abbreviated as TEOS) in a mixture of ethanol and water. The size of SiO_2 NSs can be controlled by modulating the molar ratio of TEOS, water, and ammonia. In a typical procedure, 100 mL of deionized water, 100 mL of ethanol, and 30 mL of NH_4OH were mixed in a flask and stirred for 15 min, after which a homogeneous solution formed. A 5 mL portion of TEOS was then added, and the solution was stirred for 24 h at room temperature. The resulting SiO_2 NSs were monodisperse in morphology with a typical diameter of 360−385 nm.

Preparation of Ag-Decorated SiO_2 NSs. A 0.2 g portion of the as-prepared SiO_2 NSs was dispersed in 50 mL of deionized water by ultrasonicating for 10 min. The above solution was then heated to 85 °C, at which point 0.2 M NaOH aqueous solution was added under vigorous stirring to adjust the pH to a fixed value. Following 1 h, 2 mL of $AgNO_3$ aqueous solution (0.12 M) was added to the basic solution. After stirring for an additional hour, 25 mL of ethanol was added to the mixed solution to reduce Ag^+ to Ag seeds on the surface of SiO_2 NSs. The seeding reaction was permitted to proceed for 1 h, at which point 1 mL of $AgNO_3$ aqueous solution (0.12 M) and 1 mL of trisodium citrate aqueous solution ($Na_3C_6H_5O_7$, 0.23 M) were added to grow Ag nanoparticles on SiO_2 NSs. The aforementioned growth procedure was repeated five times in order to achieve the desired Ag particle size and decoration density. The products were collected by centrifugation, washed with deionized water and ethanol, and then dried at 60 °C in air. In this work, the pH value of the seed reaction solution was adjusted to either 9.8, 10.6, 11.1, 11.3, or 12.1. The thus-obtained samples of Ag-decorated SiO_2 were denoted as SA41, SA8, SA5, SA4, and SA2, respectively.

Preparation of Individually Dispersed Ag Nanoparticles. Ag nanoparticles were prepared with a chemical reduction method.[24] In a typical procedure, ice-cooled sodium borohydride ($NaBH_4$, 10 mM, 3 mL) was added to an aqueous solution containing $AgNO_3$ (0.25 mM, 100 mL) and trisodium citrate (30 mM, 1 mL) under vigorous stirring. After 30 s, the stirring was stopped and the reaction solution was allowed to stand for 2 h, which produces individually dispersed Ag nanoparticles with an average size of 2 nm.

Preparation of N-Doped P-25 TiO_2. N-doped P-25 TiO_2 was prepared by annealing Degussa P-25 TiO_2 powder (1130 mg) in a mixed atmosphere of Ar (200 sccm) and NH_3 (10 sccm) at 500 °C for 2 h.[25] The x value of the product ($TiO_{2-x}N_x$) was about 0.28, as estimated from X-ray photoelectron spectroscopy. Note that P-25 TiO_2 is a representative photocatalyst for activity comparison when a newly designed material is demonstrated for photocatalysis applications. Since the present Ag-decorated SiO_2 absorbed light mainly in the visible range, P-25 TiO_2 was doped with N to exhibit capability in visible absorption, through which the activity comparison could be more rational.

Photocatalytic Activity Measurement. The photocatalytic performance of Ag-decorated SiO_2 NSs was evaluated by monitoring the photodegradation of methylene blue (denoted as MB) under white light irradiation (500 W xenon

dx.doi.org/10.1021/jp306555j | J. Phys. Chem. C 2012, 116, 19039−19045

lamp, with a light intensity of 175 mW/cm^2). Note that white light irradiation, which matches well natural sunlight in spectral distribution, was applied in order to demonstrate the applicability of the samples in solar energy conversion. A quartz tube with a capacity of 20 mL was used as the photoreactor vessel. Five kinds of photocatalysts, including N-doped P-25 TiO_2 powder, individually dispersed Ag nanoparticles, pristine SiO_2 NSs, Ag-loaded SiO_2 NSs, and Ag-decorated SiO_2 NS samples (SA41, SA8, SA5, SA4, SA2), were used and compared in the photodegradation of MB. A typical experiment involved adding 10 mg of photocatalyst to 20 mL of MB aqueous solution (2.0×10^{-5} M) in the photoreactor vessel. Prior to irradiation, the suspension was aerated and stirred in the dark for 30 min to reach the adsorption equilibrium of MB with photocatalyst. At certain time intervals of irradiation, 1 mL aliquots of reaction solution were withdrawn and centrifuged to remove the photocatalyst particles. The UV−visible absorption spectra of the filtrates were then acquired to measure the concentration variation of MB by recording the corresponding absorbance of the characteristic peak at 665 nm. The concentration decay data were then fitted using a pseudo-first-order model to determine the apparent rate constant of MB photodegradation. To consider the effect of surface area, the apparent photodegradation rate constant of the sample is divided by the corresponding surface area value to give the normalized photocatalytic activity that represents the photodegradation efficiency per unit surface area. Furthermore, photodegradation of MB (1.0×10^{-5} M) under natural sunlight by using Ag-decorated SiO_2 NSs as photocatalyst was also examined.

Characterizations. The morphology and dimensions of the products were examined with a high-resolution transmission electron microscope (HRTEM, JEOL JEM-3000) operated at 300 kV. The high-angle annular dark-field scanning TEM observations (HAADF STEM) were carried out on a JEOL JEM-3000 equipped with a digitally processed scanning imaging system. The crystallographic structures of the samples were studied with X-ray diffraction (XRD, Shimadzu XRD6000), and HRTEM. The compositional information was obtained with an energy-dispersive spectrometer (EDS) installed on HRTEM. The X-ray photoelectron spectra (XPS) were recorded on an Ulvac-PHI 1600 using Al Kα radiation under high-vacuum conditions. UV−visible absorption spectra were collected with a Hitachi U-3900H spectrophotometer at room temperature under ambient conditions. The Brunauer−Emmett−Teller (BET) specific surface area of the sample was estimated from the N_2 adsorption/desorption analysis. The zeta potential data were obtained using the Zetasizer Nano ZS90 (Malvern), which records the electrophoretic mobility of the sample and derives the zeta-potential value from the Smoluchowski equation.

RESULTS AND DISCUSSION

Information elucidating the composition and structure of the samples is shown in Figure 1. Figure 1a first represents the morphology of SiO_2 NSs after they were reacted with $AgNO_3$ in the seed-mediated growth process. Unlike the pristine SiO_2 NSs, which possessed a smooth surface, the $AgNO_3$-treated SiO_2 NSs were fluffy on the surface, indicating an obvious change in surface morphology. Close inspection of Figure 1a further reveals that a large quantity of nanoparticles with sizes in the range of 5−10 nm were present on the SiO_2 surface. On the basis of the evident TEM contrast between nanoparticles and NSs, we supposed that the surface-attached nanoparticles

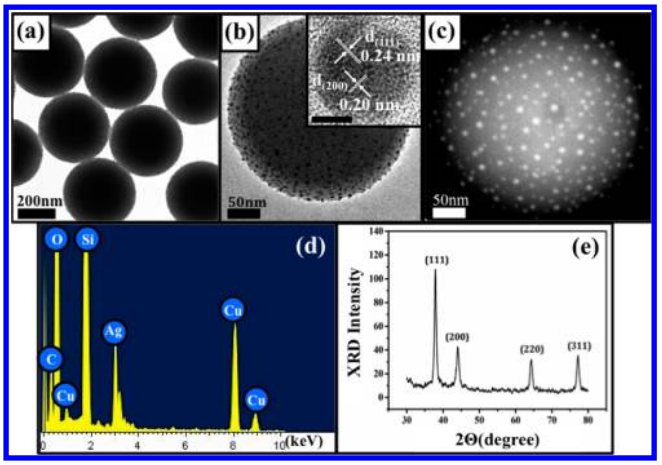

Figure 1. (a) TEM image, (b) HRTEM image, (c) HAADF STEM image, (d) TEM-EDS analysis, and (e) XRD pattern for Ag-decorated SiO_2 NSs. The inset of (b) shows the HRTEM image taken on the Ag nanoparticle region, and the scale bar is 5 nm.

were composed of Ag. Such a Ag-nanoparticle-decorated SiO_2 NS structure can be further confirmed with the corresponding HRTEM, HAADF STEM, TEM-EDS, and XRD analyses. A HRTEM image taken on the nanoparticle region is shown in the inset of Figure 1b. Interlayer spacings of 0.24 and 0.20 nm were measured and can be relatively assigned to the lattice spacings of (111) and (200) planes of fcc Ag.[26] Figure 1c displays the HAADF STEM image for a single NS. The numerous bright spots appearing on the surface of the NS may correspond to Ag nanoparticles since electrons are scattered more intensely by the heavier Ag atoms. The TEM-EDS analysis shown in Figure 1d reveals the presence of Ag along with SiO_2 in the product. In addition, the corresponding XRD pattern of Figure 1e verifies the formation of crystalline fcc Ag in the seed-mediated growth process. This result, together with the findings from HRTEM, HAADF STEM, and TEM-EDS analyses, confirms the decoration of Ag nanoparticles on SiO_2 NSs upon the seeded-mediated growth reaction.

A plausible growth mechanism for the present Ag-decorated SiO_2 NSs was proposed and illustrated in Scheme 1. In basic solution, negatively charged OH^- groups formed on the surface

Scheme 1. Schematic Illustration of the Growth Mechanism for Ag-Decorated SiO_2 NSs with Controllable Ag Particle Size and Decoration Density

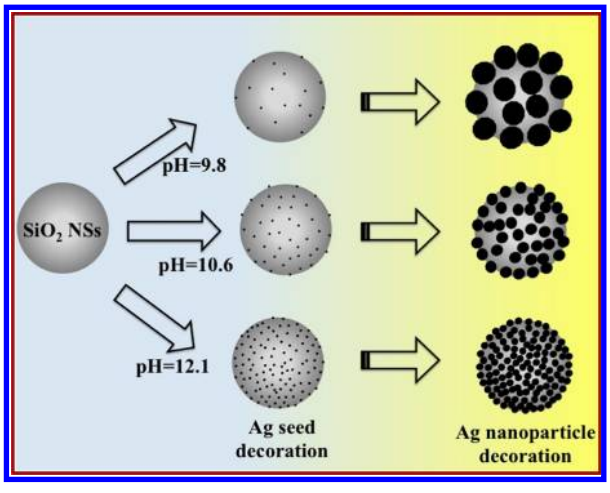

dx.doi.org/10.1021/jp306555j | J. Phys. Chem. C 2012, 116, 19039−19045

of SiO_2 NSs.[27,28] It is to such sites that positively charged Ag^+ ions electrostatically are bound. The adsorbed Ag^+ was then reduced by the added ethanol, producing Ag nuclei with a typical size of about 1 nm on the SiO_2 surface. A crystallization stage subsequently ensued as Ag deposited onto these nucleation sites, resulting in the formation of SiO_2 NSs that were decorated with Ag nanoparticles. In this work, the pH value of the seed reaction solution was modulated to study its effect on the Ag morphology of the products. Figure 2 shows

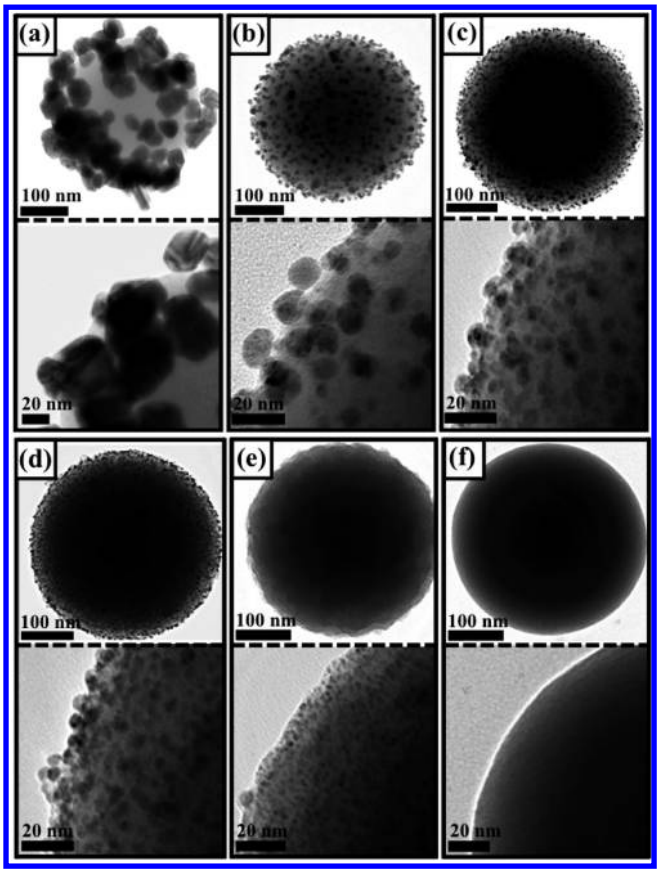

Figure 2. TEM images of Ag-decorated SiO_2 NSs prepared from seed reaction solutions of different pHs: (a) 9.8 (SA41), (b) 10.6 (SA8), (c) 11.1 (SA5), (d) 11.3 (SA4), and (e) 12.1 (SA2). The morphology of pristine SiO_2 NSs is also shown in (f) for comparison.

TEM images of Ag-decorated SiO_2 samples prepared from seed reaction solutions of different pHs. At the lowest pH employed (9.8), large Ag particles with irregular shapes were found to form on the SiO_2 surface. A gradual decrease in Ag particle size together with an apparent increase in decoration density was observed when the solution pH was raised from 9.8 to 12.1. From TEM observation, the particle size of Ag for the Ag-decorated SiO_2 samples prepared with pH values of 9.8, 10.6, 11.1, 11.3, and 12.1 was estimated to be 41.3 ± 8.1, 8.3 ± 1.3, 5.1 ± 0.7, 4.3 ± 0.5, and 2.4 ± 0.5 nm, respectively. The morphology evolution is mainly a result of the increasing amount of OH^- present on the SiO_2 surface, which leads to the generation of more Ag seed nuclei and, therefore, the production of smaller and denser Ag particles. Note that zeta-potential characterization shows that SiO_2 NSs displayed a progressive increase in net surface charge, from −60.8 to −63.4, −68.4, −72.7, and then −80 mV upon raising the solution pH from 9.8 to 10.6, 11.1, 11.3, and then 12.1. The rise in net negative charge of SiO_2 NSs may facilitate the electrostatic interaction with Ag^+, giving rise to an increased number of the adsorbed Ag^+ to promote the generation of more Ag seeds on the SiO_2 surface. Accordingly, Ag nanoparticles with reduced sizes were grown and dispersed densely on the surface of SiO_2 NSs upon raising the solution pH.

SPR is an interesting optoelectronic feature for noble metal nanoparticles, especially when a dielectric is present.[29] For example, when Ag nanoparticles are coated on the dielectric SiO_2 surface to form a core−shell-like structure, their SPR absorption can be delicately tuned by changing the Ag shell thickness as well as the SiO_2 core size.[13] To acquire the unique optical characteristics for Ag-decorated SiO_2 NSs, their SPR properties were investigated. Figure 3 shows the UV−visible

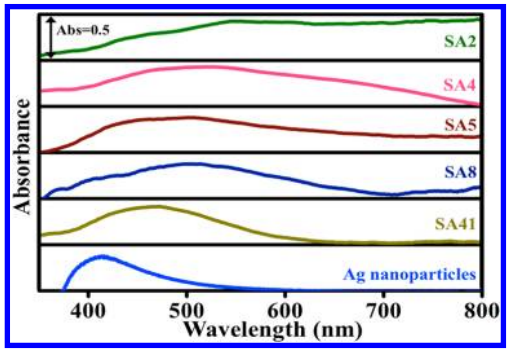

Figure 3. UV−visible absorption spectra of different Ag-decorated SiO_2 NSs. The spectrum of individually dispersed Ag nanoparticles was also included for comparison.

absorption spectra collected from the aqueous suspensions of different Ag-decorated SiO_2 samples. The result of individually dispersed Ag nanoparticles was also included for comparison. For the individually dispersed Ag, a narrow SPR absorption peak located at around 420 nm was observed. As to the Ag-decorated SiO_2 NSs, a significantly red shifted and relatively broad SPR band was recorded. Notably, the red shifting and broadening of the SPR for Ag-decorated SiO_2 NSs became more pronounced as the Ag particle size was reduced. For the Ag-decorated SiO_2 sample with the smallest Ag size (SA2 sample), the absorption band even spanned from the visible to the near-infrared region. It has been shown that the plasmon resonance oscillations on individual metal nanoparticles are coupled when they come in close proximity.[30−32] This electromagnetic coupling may enhance the polarizability of the electron cloud to lower the plasmon resonance energy, thus resulting in the red shift of SPR. With decreasing interparticle distance, a greater ease with which the electrons are polarized at the interface can be attained, leading to the more pronounced red shift in SPR absorption. Since the approach of the neighboring Ag nanoparticles with decreasing Ag particle size was evident for the present Ag-decorated SiO_2 NSs, we believed that strong electromagnetic coupling among the decorated Ag arose and was conducive to the increasingly significant red shift in SPR absorption as observed. It should be noted that the SPR red shift resulting from the interparticle coupling increases with an increase in the dielectric constant of the surrounding medium.[30] For a given interparticle distance, metal particles dispersed in a medium with a larger refractive index exhibit a higher extent of SPR red shift. Since SiO_2 has a relatively large refractive index of 1.45,[32] its combination with Ag may further boost the coupling-induced red shift of SPR. This is the main

dx.doi.org/10.1021/jp306555j | J. Phys. Chem. C 2012, 116, 19039−19045

reason why such a significant SPR red shift can be observed in the present Ag-decorated SiO_2 NSs, especially the SA2 sample. On the other hand, when the dimension of metal particles is smaller than the bulk electron mean free path, electron confinement substantially affects the dielectric function of the metal to alter the line shape of SPR.[31,33] The smaller the particles, the faster the electrons reach the surface of particles, and thus the quicker the plasmon loses the coherence due to electron scattering. As a result, the SPR bandwidth of metal particles increases with decreasing particle size. As estimated from TEM observation in Figure 2, the particle size of Ag for Ag-decorated SiO_2 samples was smaller than the electron mean free path of bulk Ag (ca. 52 nm).[34] A significant electron confinement effect hence emerged within the decorated Ag to broaden the resultant SPR line shape. In addition to the confinement effect, the interparticle coupling contributed to the SPR broadening of Ag-decorated SiO_2 NSs as well. Because of the particle interactions, an increase in local field fluctuations was presumed, giving rise to an extended range of photon energies for plasmon resonance to take place.[31]

Because Ag-decorated SiO_2 NSs absorbed light in a considerably wide range, we surmised that a sizable amount of charge carriers were generated during the photoexcitation process, which might be available for further utilization. This speculation can be confirmed by evaluating the light-energy conversion efficiency for Ag-decorated SiO_2 samples in their practical applications. Photocatalysis is a valuable approach to practically convert light into chemical energy. To investigate the potential as a photocatalyst for the present Ag-decorated SiO_2 NSs, we performed a series of photocatalysis experiments. MB, a typical dye that can be decomposed by reacting with charge carriers following the irradiation on photocatalysts, was used as the test pollutant. Five kinds of photocatalysts, including N-doped P-25 TiO_2 powder, individually dispersed Ag nanoparticles, pristine SiO_2 NSs, Ag-loaded SiO_2 NSs (denoted as SiO_2@Ag), and Ag-decorated SiO_2 NSs (SA41, SA8, SA5, SA4, SA2), were used for MB photodegradation under the same experimental conditions. Note that SiO_2@Ag was prepared by simply mixing pristine SiO_2 NSs with individually dispersed Ag nanoparticles, which results in a random distribution of Ag nanoparticles around SiO_2 NSs. To offer a fair comparison, an identical quantity of Ag to that of the SA2 sample was employed in SiO_2@Ag preparation. The comparative results are shown in Figure 4a, from which several points can be observed. First, experiment in the absence of photocatalyst showed a slight degradation of MB, indicating a minor self-photolysis of MB molecules under white light illumination. This self-photolysis effect further accounted for the slight extent of MB degradation observed in individually dispersed Ag nanoparticles and pristine SiO_2 NSs. Second, the photocatalytic efficiency of Ag-decorated SiO_2 NSs was enhanced with decreasing Ag particle size, mainly resulting from the broader SPR absorption observed for the sample with a smaller Ag size. As the SPR absorption was broadened, the light-harvesting efficiency of the sample was improved, generating more charge carriers to favor the subsequent photocatalysis. Consequently, a better photocatalytic activity was observed for the sample with a smaller Ag particle size. Although the SPR absorption of SA41 was not much different than that of Ag nanoparticles, the firmly immobilized Ag of SA41 avoided possible particle agglomeration, which may further cause activity depression during photocatalysis operation. As a consequence, SA41 performed much better than Ag

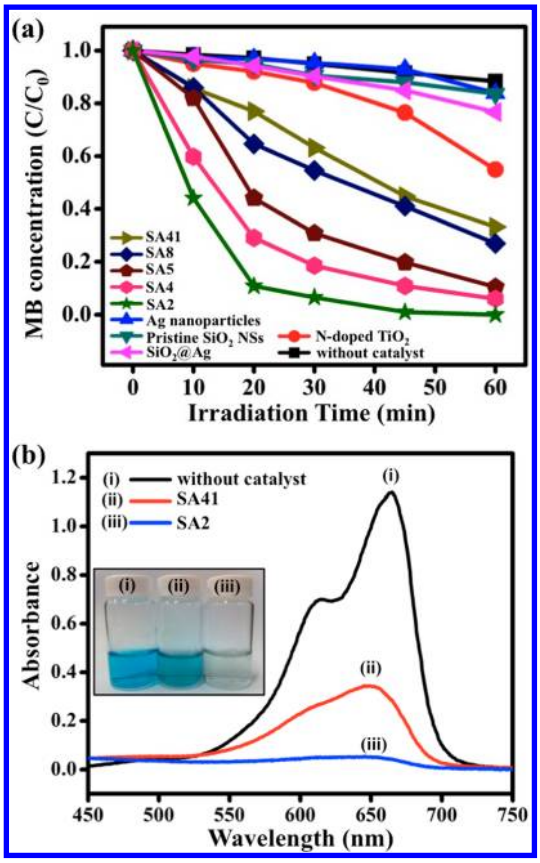

Figure 4. (a) C/C_0 versus irradiation time plots for MB photodegradation without any catalyst and in the presence of five kinds of relevant samples. (b) Absorption spectra of MB solutions following a 3 h exposure to daytime sunlight without any catalyst and in the presence of Ag-decorated SiO_2 NSs (SA41 and SA2). Inset shows the corresponding solution color.

nanoparticles did in MB photodegradation. Third, as compared with N-doped P-25 TiO_2, the five Ag-decorated SiO_2 samples all exhibited superior photocatalytic performance under white light illumination. This outcome was ascribed to the conspicuous SPR absorption of the decorated Ag nanoparticles that can induce the generation of abundant charge carriers for participation in MB degradation. Similar results were reported for the cases of Ag nanoparticles on polymer and oxide supports.[10,11] In those cases, the SPR of Ag heats the electrons and excites them from the outermost sp bands to higher energy states, simultaneously leaving photogenerated holes at the sp bands. Both the photoexcited electrons and the holes can participate in redox reactions to decompose organic pollutants. Moreover, the interband transition invoked by ultraviolet irradiation may generate additional holes at the inner d band of Ag, which are also available for oxidation utilization. In the present case, by reacting with photogenerated holes, MB undergoes typical photooxidation to get decomposed. On the other hand, since MB is a cationic dye with a relatively low reduction potential of +0.01 V vs NHE, it may readily accept photoexcited electrons from Ag and get degraded.[35,36] Lastly, the SiO_2@Ag sample did not perform as well as Ag-decorated SiO_2 did, presumably owing to less contact of Ag with SiO_2 in SiO_2@Ag. Because of the limited contact between Ag and SiO_2, poor dispersion of Ag nanoparticles on the SiO_2 surface was expected for the SiO_2@Ag sample, which, in turn, retards the interparticle coupling of Ag to shorten the energy range of the

dx.doi.org/10.1021/jp306555j | J. Phys. Chem. C 2012, 116, 19039−19045

plasmon resonance. Under this circumstance, a smaller amount of charge carriers were produced in SiO_2@Ag upon SPR excitation and a lower photocatalytic activity was thereby attained. This demonstration further emphasizes the beneficial effect of particle decoration as well as interparticle coupling on the SPR-mediated photocatalytic performance of Ag.

To quantitatively compare the photocatalytic performance of different Ag-decorated SiO_2 samples, the apparent rate constant for MB photodegradation (k_{MB}) was computed using the pseudo-first-order approximation. By use of the results of Figure 4a, we obtained k_{MB} values of 3.4, 4.0, 6.0, 9.8, and 21.0 min^{-1} g^{-1} for SA41, SA8, SA5, SA4, and SA2, respectively. It might be argued that the observed difference in photocatalytic activity among the five Ag-decorated SiO_2 samples emanated from the variation in Ag content.[9] To clarify this issue, we performed XPS measurements to estimate the amount of Ag in each sample. XPS characterization shows that the content of Ag for different Ag-decorated SiO_2 samples was commensurate, roughly 26.5, 31.6, 31.7, 31.0, and 31.0 wt % for SA41, SA8, SA5, SA4, and SA2, respectively. This result signifies that the enhancement in photocatalytic activity for Ag-decorated SiO_2 NSs with smaller Ag sizes was not due to the presence of a higher concentration of Ag in the reaction medium. It might also be argued that the larger surface area expected for the sample with a smaller Ag size was the leading cause for the performance improvement. This argument is rational since a larger surface area does offer more active sites for photocatalytic reactions. To separate the surface area effect from the intrinsic activity, the k_{MB} of the sample was further normalized with the corresponding specific surface area.[37] The BET surface area (S_{BET}) of SA41, SA8, SA5, SA4, and SA2 was measured to be 6.9, 8.0, 10.0, 15.0, and 19.1 m^2 g^{-1}, respectively. Dividing k_{MB} by S_{BET}, respectively, gives the normalized rate constant of MB photodegradation (k'_{MB}) as 0.49, 0.50, 0.60, 0.65, and 1.10 min^{-1} m^{-2}. Obviously, the increasing trend of k'_{MB} still continued for the sample as the Ag particle size was reduced. This observation shows that Ag with a reduced size favored the photocatalysis of the sample in terms of other factors besides surface area. Since the significantly red shifted and relatively broad SPR was the main consequence of the reduced Ag size, which may effectively improve the carrier generation efficiency, we ascribed the k'_{MB} enhancement of Ag-decorated SiO_2 NSs with decreasing Ag size to the SPR mediation. To further explore the applicability of Ag-decorated SiO_2 NSs in a more practical situation, their photocatalytic performance under natural sunlight was evaluated. In this experiment, two representative samples, SA41 and SA2, were tested and compared. As illustrated in Figure 4b, after exposure to 3 h of daytime sunlight, MB was totally degraded by using SA2, accompanied with an obvious decoloration of the resultant solution. In contrast, SA41 only decomposed 70% of MB under the same experimental conditions. This activity difference, which is in conformity with the observation from Figure 4a, was due to the different SPR absorption ranges between SA2 and SA41. Most importantly, this result shows that the present Ag-decorated SiO_2 NSs, especially the SA2 sample, can be used as highly efficient photocatalysts that may practically harvest energy from sunlight.

CONCLUSIONS

In conclusion, a seed-mediated growth approach was developed to prepare Ag-decorated SiO_2 NSs. The Ag particle size and decoration density of the products can be readily controlled by adjusting the pH value of the seed reaction solution. The as-prepared Ag-decorated SiO_2 NSs showed a significantly red shifted and relatively broad SPR absorption when compared with the individually dispersed Ag nanoparticles. The red shifting and broadening of the SPR for Ag-decorated SiO_2 NSs became more pronounced as the Ag particle size was reduced, presumably due to the increasingly significant electromagnetic coupling among the decorated Ag. The photocatalytic efficiency of Ag-decorated SiO_2 NSs was enhanced with decreasing Ag particle size, mainly resulting from the broader SPR absorption observed for the sample with a smaller Ag size. As compared with N-doped P-25 TiO_2 and individually dispersed Ag nanoparticles, the as-synthesized Ag-decorated SiO_2 NSs exhibited superior photocatalytic performance toward MB photodegradation, attributable to the conspicuous SPR absorption of the decorated Ag that can induce the generation of abundant charge carriers for participation in MB degradation. Furthermore, the result of the performance evaluation under natural sunlight shows that Ag-decorated SiO_2 NSs can be used as highly efficient photocatalysts that may practically harvest energy from sunlight. The present Ag-decorated SiO_2 NSs may find potential use for unique photocatalytic applications, for example, to drive chemical reactions currently using Ag catalysts at ambient temperature under light illumination.[38] The current study opens a new avenue toward the design of distinctive chemical transformations that are driven by both thermal flux and photon energy sources.[12] The findings from this work also shed light on the development of composite plasmonic metal/semiconductor photocatalyst systems in which SPR mediation and electronic effects[39,40] synergistically regulate the carrier generation and charge transfer to enhance the photoactivities.

AUTHOR INFORMATION

Corresponding Author

*E-mail: hcshih@mx.nthu.edu.tw (H.-C.S.), yhsu@cc.nctu.edu.tw (Y.-J.H.).

Author Contributions

⊥These authors contributed equally.

Notes

The authors declare no competing financial interest.

ACKNOWLEDGMENTS

This work was financially supported by the National Science Council of the Republic of China (Taiwan) under grants NSC-100-2622-E-034-001-CC2 (H.-C.S.) and NSC-100-2113-M-009-004 (Y.-J.H.).

REFERENCES

(1) Lewis, N. S. *Science* **2007**, *315*, 798−801.
(2) Malato, S.; Fernández-Ibáñez, P.; Maldonado, M. I.; Blanco, J.; Gernjak, W. *Catal. Today* **2009**, *147*, 1−59.
(3) Hu, X.; Li, G.; Yu, J. C. *Langmuir* **2010**, *26*, 3031−3039.
(4) Chen, X.; Liu, L.; Yu, P. Y.; Mao, S. S. *Science* **2011**, *331*, 746−750.
(5) Xiong, S.; Xi, B.; Qian, Y. *J. Phys. Chem. C* **2010**, *114*, 14029−14035.
(6) Zhang, H.; Zhu, Y. *J. Phys. Chem. C* **2010**, *114*, 5822−5826.
(7) Thibert, A.; Frame, F. A.; Busby, E.; Holmes, M. A.; Osterloh, F. E.; Larsen, D. S. *J. Phys. Chem. Lett.* **2011**, *2*, 2688−2694.
(8) Holmes, M. A.; Townsend, T. K.; Osterloh, F. E. *Chem. Commun.* **2012**, *48*, 371−373.

(9) Wu, Z.-C.; Zhang, Y.; Tao, T.-X.; Zhang, L.; Fong, H. *Appl. Surf. Sci.* **2010**, *257*, 1092−1097.
(10) Chen, X.; Zheng, Z.; Ke, X.; Jaatinen, E.; Xie, T.; Wang, D.; Guo, C.; Zhao, J.; Zhu, H. *Green Chem.* **2010**, *12*, 414−419.
(11) Ke, X.; Ribbens, S.; Fan, Y.; Liu, H.; Cool, P.; Yang, D.; Zhu, H. *J. Membr. Sci.* **2011**, *375*, 69−74.
(12) Linic, S.; Christopher, P.; Ingram, D. B. *Nat. Mater.* **2011**, *10*, 911−921.
(13) Lin, Q.; Sun, Z. *J. Phys. Chem. C* **2011**, *115*, 1474−1479.
(14) Jiang, Z.; Liu, C. *J. Phys. Chem. B* **2003**, *107*, 12411−12415.
(15) Kobayashi, Y.; Salgueiriño-Maceira, V.; Liz-Marzán, L. M. *Chem. Mater.* **2001**, *13*, 1630−1633.
(16) Zhu, M.; Qian, G.; Hong, Z.; Wang, Z.; Fan, X.; Wang, M. *J. Phys. Chem. Solids* **2005**, *66*, 748−752.
(17) Liu, T.; Li, D.; Yang, D.; Jiang, M. *Colloids Surf., A* **2011**, *387*, 17−22.
(18) Tang, S.; Tang, Y.; Gao, F.; Liu, Z.; Meng, X. *Nanotechnology* **2007**, *18*, 295607.
(19) Pol, V. G.; Srivastava, D. N.; Palchik, O.; Palchik, V.; Slifkin, M. A.; Weiss, A. M.; Gedanken, A. *Langmuir* **2002**, *18*, 3352−3357.
(20) Tang, S.; Tang, Y.; Zhu, S.; Lu, H.; Meng, X. *J. Solid State Chem.* **2007**, *180*, 2871−2876.
(21) Quang, D. V.; Sarawade, P. B.; Hilonga, A.; Kim, J.-K.; Chai, Y. G.; Kim, S. H.; Ryu, J.-Y.; Kim, H. T. *Colloids Surf., A* **2011**, *389*, 118−126.
(22) Chen, Y.; Kim, H. *Mater. Lett.* **2007**, *61*, 5040−5043.
(23) Cassagneau, T.; Caruso, F. *Adv. Mater.* **2002**, *14*, 732−736.
(24) Lu, L.; Kobayashi, A.; Tawa, K.; Ozaki, Y. *Chem. Mater.* **2006**, *18*, 4894−4901.
(25) Yang, T.-T.; Chen, W.-T.; Hsu, Y.-J.; Lin, T.-Y.; Lin, T.-W. *J. Phys. Chem. C* **2010**, *114*, 11414−11420.
(26) For bulk fcc Ag, $d(111)$ = 0.235 nm and $d(200)$ = 0.204 nm from JCPDS 87-0719.
(27) Pu, Y.-C.; Chen, Y.-C.; Hsu, Y.-J. *Appl. Catal., B* **2010**, *97*, 389−397.
(28) Jean, R.-D.; Chiu, K.-C.; Chen, T.-H.; Chen, C.-H.; Liu, D.-M. *J. Phys. Chem. C* **2010**, *114*, 15633−15639.
(29) Kelly, K. L.; Coronado, E.; Zhao, L. L.; Schatz, G. C. *J. Phys. Chem. B* **2003**, *107*, 668−677.
(30) Jain, P. K.; El-Sayed, M. A. *Nano Lett.* **2008**, *8*, 4347−4352.
(31) Sancho-Parramon, J. *Nanotechnology* **2009**, *20*, 235706.
(32) Jain, P. K.; El-Sayed, M. A. *J. Phys. Chem. C* **2007**, *111*, 17451−17454.
(33) Haiss, W.; Thanh, N. T. K.; Aveyard, J.; Fernig, D. G. *Anal. Chem.* **2007**, *79*, 4215−4221.
(34) Kaniyankandy, S.; Nuwad, J.; Thinaharan, C.; Dey, G. K.; Pillai, C. G. S. *Nanotechnology* **2007**, *18*, 125610.
(35) Kobasa, I. M.; Tarasenko, G. P. *Theor. Exp. Chem.* **2002**, *38*, 255−258.
(36) Chen, Y.-C.; Pu, Y.-C.; Hsu, Y.-J. *J. Phys. Chem. C* **2012**, *116*, 2967−2975.
(37) Yu, J.; Zhang, J. *Dalton Trans.* **2010**, *39*, 5860−5867.
(38) Christopher, P.; Xin, H.; Linic, S. *Nat. Chem.* **2011**, *3*, 467−472.
(39) Kumar, M. K.; Krishnamoorthy, S.; Tan, L. K.; Chiam, S. Y.; Tripathy, S.; Gao, H. *ACS Catal.* **2011**, *1*, 300−308.
(40) Torimoto, T.; Horibe, H.; Kameyama, T.; Okazaki, K.; Ikeda, S.; Matsumura, M.; Ishikawa, A.; Ishihara, H. *J. Phys. Chem. Lett.* **2011**, *2*, 2057−2062.